Conversion of Lavandula distilled straws into high-quality solid fuel: effect of hydrothermal carbonization conditions on fuel characteristics

Xin Li
Universite Cote d'Azur
Sumeyra Seniha Baran
Universite Cote d'Azur
François Orange
Universite Cote d'Azur
Erik Bonjour
Institut des Sciences Analytiques
Patrick Jame
Institut des Sciences Analytiques
Alice Mija
Universite Cote d'Azur
Claire Lomench
Universite Cote d'Azur
Pavel Kuzhir
Universite Cote d'Azur
Charlotte Hurel (charlotte.hurel@unice.fr)
Université Côte d'Azur https://orcid.org/0000-0001-6187-6354

Research Article

Keywords: hydrothermal carbonization, hydrochar, biomass waste, solid fuel, lavandin, distilled straws

Posted Date: May 16th, 2022

DOI: https://doi.org/10.21203/rs.3.rs-1637339/v1

Abstract

Lavandin hydrochars obtained by hydrothermal carbonization (HTC) of *Lavandula* distilled straw (LDS) have been studied as an eco-friendly and economical valorization route of residual biomass from cosmetic industry into solid fuels. The critical parameters of the HTC process (temperature and retention time) were normalized to severity factor (SF). Proximate and ultimate analysis, microscopy and thermal analysis were used to characterize hydrochars surface, combustion behavior and kinetics as a function of SF, and to compare them with those of the raw lavandin sample. Results showed that preparation of lavandin hydrochars in temperature and retention time conditions providing SF close to 6 seemed to be the best compromise since under these conditions, the combustion performance of the hydrochar was close to the bituminous coal and lignite.

Introduction

France is a world leader in terms of perfume industry exportations. Perfume plants cultivation and transformation have been performed since the 17th Century, mainly in the South East Region of France. Grasse (Alpes Maritimes, France) is the international capital of perfume, and concentrates most of the national industrial activity related to perfume and cosmetics. The *Lavandula* genus (lavender and lavandin), native from the Mediterranean area, is cultivated in Provence on around 20,000 ha of crops. Each year, more than 1,000 tons of *Lavandula* essential oil are locally produced by water steam distillation. Lavandin essential oil production predominates over lavender due to its higher yield (100 kg/ha vs. 15 kg/ha for lavender) and its lower price, making it of interest for industry [1]. Nevertheless, due to the low concentration of essential oil in the crops, a huge amount of plant is distilled, and consequently a huge amount of solid residual biomass is generated (20,000 tons in France, representing 90% of the worldwide generation).

Considering the nowadays challenges regarding reduction of waste volume and reduction of greenhouse gas generation, environmental and ecological issues of distilled straws from perfume industry are of the major concern. Indeed, more than 40% of distilled straws are discarded. Possible valorization routes of medicinal and aromatic plants biomass have been compiled in a recent review by Saha and Basak [2]. Among them, development of supplementary extractions to isolate molecules of pharmaceutic interest such as bioactive phytochemicals, bioactive phenolic antioxidants from the residual biomass were suggested to be more deeply investigated. Although this alternative seems very promising, it does not contribute to substantially decrease the residual biomass volume. Digestion of residual biomass by microbes or bacteria to produce biogas or enzymes also attracted high attention since the production costs are low. Valorization of residual biomass as biofuels [3, 4], biogas [5, 6], biosorbent [7, 8], biochar [9, 10] and biopesticides [11, 12] was also investigated, as well as reuse of residual biomass as soil amendment [13, 14], organic mulch [15] and animal feed [16].

Concerning *Lavandula* distilled straw (LDS) valorization, utilization as feedstock for producing high-added value compounds (antioxidants, aroma), fungal oxidative enzymes to improve decomposition of lignocellulose into biofuel[17], or conversion into mycelium-based biomaterials[18] have been proposed as interesting issues. The use of LDS as a co-composting material mixed with cattle manure and barley straw has also been recently investigated and results showed that organic matter degradation was accelerated in the presence of LDS despite some negative aspects such as increased C/N ratio and a decrease in germination index have been pointed out [19]. The major drawback of LDS biomass is the high amount of residual water after distillation, making pyrolysis/gasification processes to transform biomass into gas, oil and/or coal not adapted and not beneficial (i) to the overall economic balance in terms of energy consumption and (ii) to the greenhouse gas generation. To overcome this main drawback, treatment of wet biomass such as LDS by hydrothermal carbonization (HTC) seems a promising technique adapted to transform biomass into solid fuel, with a low environmental impact due to the low emission of greenhouse effect gas and the low energy consumption [20].

HTC is performed in a closed vessel, under self-generated pressure (2–10 MPa) obtained by heating under moderate temperature (180–250°C) for several hours. During HTC, reaction paths resulted in dehydration, decarboxylation, aromatization, hydrolysis and condensation, but the exact mechanisms are still under elucidation[21]. Factors affecting HTC

process are (i) retention time (i.e duration of thermal treatment), (ii) temperature, (iii) water to biomass ratio, and (iv) biomass composition [22]. Among these factors, temperature and retention time are the most influencing ones, followed by biomass composition. Biomass conversion resulted in carbon rich materials called hydrochars, with properties depending on the thermoconversion conditions: when high temperatures were applied, solid fuel quantity was low but it presented high carbon content and elevated higher heating value (HHV). In contrast, when low temperatures were applied, the solid fuel production was higher due to an incomplete decomposition of cellulose and hemicellulose. The solid/liquid/gas yield ratio is mainly affected by the retention time, and the solid fuel density is directly affected by the pressure [22].

Many kinds of biomass have been investigated under HTC: wood and woody biomass [23, 24], agricultural biomass [25], aquatic biomass [26], human [27] and animal [28] biowaste, industrial biomass [29]; alone or mixed with other varieties of biomass [30, 31]. To our knowledge, wet biomass produced from perfume and cosmetic industry from South-East of France are in majority pyrolyzed in treatment units far away from their production site. Their valorization as solid fuel after HTC treatment has not been investigated whereas it could be the most adapted conversion route from economic and environmental perspectives. This valorization is the objective of this work.

To reach this objective, HTC conditions were investigated under a constant water to biomass ratio and variables retention time (from 1 to 20 hours) and temperatures (from 180 to 260°C) in order to get severity factors (SF) (single variable combining temperature and retention time conditions) ranging from 4.74 to 7.79. Proximate and ultimate analysis, scanning electron microscopy (SEM), attenuated total reflectance infrared spectroscopy (ATR-FTIR) were performed on lavandin sample and hydrochars for characterization. Then, combustion behavior and combustion kinetics were studied by the help of thermogravimetric analysis (TGA), in order to evaluate the influence of severity factor (and consequently HTC conditions) on the thermal properties of hydrochars, in the context of their utilization as solid fuel.

Materials And Methods

Lavandin sample and hydrochars preparation

Lavandin was collected in the Alpes-Maritimes tdepartement (GPS coordinates: 43.765533; 7.345123), France. Lavandin sample was grinded by using a domestic blender and sieved to reach particle size between 125 and 500 µm by using a FRITSCH ANALYSETTE vibrating sieve.

The hydrothermal carbonization (HTC) of the lavandin was performed in sealed reactors (Series 4560 Mini Reactors, Parr Instrument Company) equipped with stainless steel vessels, polytetrafluoroethylene (PTFE) flat gasket and mechanical stirring devices. A constant initial solid/liquid ratio (S:L) was chosen for all HTC experiments. For that, 20 g of lavandin and 100 mL deionized water were inserted in the reactor in order to get S:L ratio of 1:5. The reactor was wrapped in an electric furnace, heated to the desired temperature (180–260°C), and maintained at the constant temperature for several hours (1–20 h). When the desired retention time was reached, the reactor was removed from the electric furnace to cool naturally at room temperature. HTC reaction occurred under self-generated pressure. The slurry after the HTC reaction was filtered by pre-weighed filter paper; the solid phase was separated and dried overnight in an oven at 105°C and manually grinded. Table 1 shows details of samples preparation during HTC. Raw lavandin and its corresponding hydrochars were abbreviated as L and LHx-y, respectively. The retention time (in hours) and temperature (in °C) were represented by x and y, respectively.

Table 1
Details of sample preparation during HTC

Sample ID	Retention time (h)	Temperature (°C)	SF	S:L
L	0	NA	NA	NA
LH1-220	1	220	5.31	1:5
LH2-220	2	220	5.61	1:5
LH4-220	4	220	5.91	1:5
LH8-220	8	220	6.21	1:5
LH20-220	20	220	6.61	1:5
LH4-180	4	180	4.74	1:5
LH4-200	4	200	5.32	1:5
LH4-240	4	240	6.50	1:5
LH20-200	20	200	6.02	1:5
LH20-240	20	240	7.20	1:5
LH20-260	20	260	7.79	1:5

Temperature and retention time being the most important variables in HTC treatments, it is possible to combine them into a single factor (R_0), easy to use in order to display trends [32]:

$$R_0 = t \times exp\left(\frac{T-100}{14.75}\right) \text{ (Eq. 1)}$$

with t being the retention time (min), T the temperature (°C) and 14.75 is a fitted parameter inversely proportional to the activation energy of the hydrolytic process, corresponding to an increase of the reaction rate by a factor of 2 when the temperature is increased by 10°C [33]. The equation is based on the assumption that the reaction is hydrolytic and that the overall conversion follows first order kinetics and Arrhenius temperature behavior [34]. The severity factor (SF) corresponds to $logR_0$.

Proximate analysis

The proximate analysis including moisture, ash, and volatile matter contents of raw lavandin and its hydrochars were determined by using a thermogravimetric analyzer (Mettler Toledo TGA2 Star System), based on American Society for Testing and Materials (ASTM) E871-82 [35], ASTM E1755-01 [36] and ASTM E872-82 [37] methods, respectively. The fixed carbon content percentage was calculated from the difference between 100 and the sum of moisture, ash and volatile matter content percentages. From proximate analysis, fuel ratio and hydrochar yield were calculated.

Fuel ratio = $\frac{Fixedcarbon(\%wt)}{volatilematter(\%wt)}$ (Eq. 2)

Hydrochar yield (%) = $\frac{driedhydrocharmass}{driedbiomassmass} \times 100.$ (Eq. 3)

Elemental Analysis

Carbon, hydrogen measurements were performed on a homemade Carbon/Hydrogen elemental micro-analyzer (ISA, CNRS, Villeurbanne). About 1.5 mg of sample weighted in silver cups dropped into a flow of 50 mL min^{-1} of pure oxygen into a unit combustion hold at 1050°C and half filled with CuO. Carbon and hydrogen were transformed into carbon dioxide (CO_2) and

water (H_2O) respectively, prior to be measured using a CO_2/H_2O non-dispersive infrared detector. The precision has been evaluated at +/- 0.30% for carbon and hydrogen.

Nitrogen analyses was taken into account using a homemade nitrogen elemental Micro-analyzer (ISA, CNRS Villeurbanne). Sample weighted in silver cup fall in a similar unit combustion previously described where nitrogen has been turned into nitrogen oxide in a flow of helium and oxygen. The gases pass through a copper wire tube hold at 450°C where nitrogen oxide were reduced in nitrogen N_2 followed by a CO_2/H_2O trap. The quantification of N_2 resulting has been done on a TCD Thermo Conductibility Detector. Precision has been established < 0.20%.

Sulfur determination has been performed using a carbon sulfur SC144 analyzer (LECO, St Joseph, USA). About 10 mg of samples has been introduced into a horizontal combustion unit maintained at 1350°c where carbon and Sulphur are turned into CO_2 and SO_2 prior to be quantified using CO_2 and SO_2 non-dispersive infrared cells. Precision on sulfur analysis was evaluated at 0.10%.

Calorific values (HHV) were calculated from elemental analysis according to Channiwala et al. (2002) [38].

$$HHV = 0.349C + 1.1783H + 0.1005S - 0.1034O - 0.0015N - 0.0211Ash \text{ (Eq. 4)}$$

with HHV in (MJ kg^{-1}), C, H, S, O, N and Ash in (% wt). According to Eq. 4, high HHV value is correlated to high carbon, sulfur and hydrogen contents and low oxygen, nitrogen and ash content.

Energy yield (%) was calculated from HHV and hydrochar yield.

$$\text{Energy yield} = \frac{HHV_{hydrochar}}{HHV_{biomass}} \times hydrocharyield \text{ (Eq. 5)}$$

SEM, ATR-FTIR

Surface morphologies of raw lavandin and its hydrochars were investigated with Scanning Electron Microscopy (SEM). Observations were performed with a Tescan Vega3 SEM, using secondary electron with a 5 kV voltage and in high vacuum mode with various magnifications. Particle size distribution was determined from SEM images of each sample. At least 30 to 50 particles with clear and easily distinguishable outlines were selected and measured using ImageJ free open source software [39].

Fourier-Transform Infrared (FT-IR) spectrometer (Nicolet iS50 FT-IR spectrometer with a GladiATR single diamond attenuated total reflectance system (PIKE Technologies, Inc.) was used to ascertain the change of functional groups and chemical bonds on the surfaces of raw lavandin and its hydrochars. For each sample, 32 scans were performed, in the wavenumber range between 400 and 4000 cm^{-1} with a resolution of 4 cm^{-1}.

Thermodegradation of lavandin and hydrochars samples

Thermodegradation of lavandin and its hydrochars was performed by Mettler Toledo TGA2 (operated with Star software) under constant air flow (150 mL min^{-1}) at temperatures between 25-1000°C with constant heating rate (10°C min^{-1}), in order to evaluate the combustion behavior of the samples. Ignition (T_i) and burnout (T_b) temperatures were determined according to the intersection method and conversion method, respectively, as suggested by Lu and Chen[40]. Ignition temperature corresponds to the minimum temperature at which a fuel spontaneously ignite without external source of ignition, and the burnout temperature corresponds to the temperature at which 99% of the initial biomass is consumed. Both parameters are crucial for evaluating fuel properties and conditions for a safe storage and transportation.

Combustibility index (S) was calculated as follows:

$$S = \frac{\left(\frac{dw}{dt}\right)_{max}\left(\frac{dw}{dt}\right)_{mean}}{T_b \times T_i^2}$$ (Eq. 6)

where $\left(\frac{dw}{dt}\right)_{max}$ and $\left(\frac{dw}{dt}\right)_{mean}$ were the maximum mass loss rate (% min^{-1}) and the average loss rate ((% min^{-1}) from DTG curves, respectively, T_b and T_i the burnout and ignition temperatures (°C) respectively. This index is used as a criterion for fuel combustion performance. It includes the ease of ignition, the burning velocity and the burnout temperature. S index higher than 2 x 10^{-7} $\%^2$ min^{-2} $°C^{-3}$ correponded to interesting material for combustion purposes [41].

Calculation of kinetic parameters [42]

The kinetics of combustion process is given by:

$$\frac{d\alpha}{dt} = kf(\alpha)$$ (Eq. 7)

$$f(\alpha) = (1-\alpha)^n$$ (Eq. 8)

$$\alpha = \frac{(m_i - m)}{(m_i - m_f)}$$ (Eq. 9)

With α the thermal conversion factor of the sample at a given time (t) calculated from TG/DTG curves: m_i,m and m_f are initial, instantaneous and final mass of sample, respectively, n is the order of reaction, and k is the rate constant determined from Arrhenius equation:

$$k = Ae^{\left(-\frac{E}{RT}\right)}$$ (*Equation 10*)

Where $A$is the pre-exponential factor (min^{-1}), E is the activation energy (J mol^{-1}), R is the gas constant (8.314 J mol^{-1} K^{-1}), T is the temperature (K).

Combination of Eq. 7 with Eq. 10 gives:

$$\frac{d\alpha}{f(\alpha)} = Ae^{\left(-\frac{E}{RT}\right)}dt$$ ² (Eq. 11)

Heating rate corresponds to $\beta = \frac{dT}{dt}$, Eq. 11 becomes:

$$\frac{d\alpha}{f(\alpha)} = \frac{A}{\beta}e^{\left(-\frac{E}{RT}\right)}dT$$ (Eq. 12)

Integral of Eq. 12 is:

$$\int_0^{\alpha}\frac{d\alpha}{f(\alpha)} = \int_{T_0}^{T}\frac{A}{\beta}e^{\left(-\frac{E}{RT}\right)}dT = G(\alpha)$$ (Eq. 13)

Coats-Redfern approximation[43] gives:

$$ln\frac{G(\alpha)}{T^2} = ln\left(\frac{AR}{\beta E}\left(1-\frac{2RT}{E}\right)\right) - \frac{E}{RT}$$ (Eq. 14)

Considering that E > 10 kJ mol^{-1} and T < 500 K, $\frac{RT}{E} \ll 1$, Eq. 14 simplifies as:

$ln\frac{G(\alpha)}{T^2} = ln\frac{AR}{\beta E} - \frac{E}{RT}$ (Eq. 15)

For the first order reaction (n = 1), $G(\alpha) = -\ln(1-\alpha)$.

For the order different to one, $G(\alpha) = \frac{1-(1-\alpha)^{1-n}}{1-n}$.

The linear regression equation of plot of $ln\frac{G(\alpha)}{T^2}$ vs $\frac{1}{T}$ allows the determination of activation energy (E) and pre-exponential factor (A) (data not shown).

Results And Discussion

Proximate and elemental analysis of lavandin and hydrochars

Table 2 presents proximate and elemental analysis of lavandin and its hydrochars. Moisture content of lavandin sample was initially low (< 3% wt) compared to other biomass [44]. After HTC treatment, moisture content decreased below 1%. Volatile matter in lavandin sample was near 81% and decreased in hydrochars as retention time increased and/or as temperature increased. On the contrary, fixed carbon, initially low for lavandin (8.55%) increased in hydrochars as the retention time and/or the temperature increased. Compensation of volatile matter decrease by fixed carbon increase is represented by the fuel ratio. An increase in fuel ratio indicates that fixed carbon increases and volatile matter decreases. Hence fuel ratio can be used as one of the determining parameters for evaluation of biofuel quality. As an example, the fuel ratio of hydrochars obtained from rice husk and coconut husk were in the range 0.66–0.86 and 0.43–0.62 [45], the fuel ratio of hydrochars obtained from filamentous algae (*H. reticulatum*) and microalgae (*C. vulgaris*) were 0.13–0.2 and 0.12–0.16, respectively [46]. Fuel ratio was 0.11 for lavandin and it ranged from 0.3 to 0.69 for hydrochars. Fuel ratio of lavandin hydrochars were on the same order of magnitude than fuel ratio for rice and coconut husks hydrochars [43] meaning that hydrochars were better solid fuels than raw biomass. Evolution of fuel ratio depending on severity factor in presented on Fig. 1 (a), and is compared to fuel ratio from Liu et al. [47] for coconut fibers and eucalyptus leaves hydrochars obtained for the same S:L conditions than the one used in this study and severity factors were ranging from 4.42 to 9.57. Fuel ratios were in the same order of magnitude for lavandin hydrochars, coconut fibers hydrochars and eucalyptus leaves hydrochars. Fuel ratio linearly increased with severity factor for the three hydrochars. The growth rate was the same for lavandin and coconut fibers hydrochars, and it was slightly lower for eucalyptus leaves. Evolution of fuel ratio indicated that at the highest severity factor values, fixed carbon content was the highest and volatile matter content was the lowest. For lavandin hydrochars, sample LH20-260 presented the best fuel properties, compared to other lavandin hydrochars. Ash content was around 7.6% in lavandin and it was low for all lavandin hydrochars (around 5%), indicating a low amount of combustion residues. Regarding ash content, lavandin hydrochars are better fuels than lavandin. From ultimate analysis, carbon content in lavandin hydrochars increased as severity factor increased, while oxygen content decreased as severity factor increased. Nitrogen and hydrogen variations were less noticeable (Fig. 1 (b)). Calculated HHV values ranged from 21.43 MJ kg^{-1} for lavandin to 30.77 MJ kg^{-1} for lavandin hydrochar. These HHV values were higher than HHV obtained from sewage sludge hydrochar [48, 49] (around 10–15 MJ kg^{-1}) but were in the same order of magnitude than hydrochars from miscanthus, eucalyptus bark, empty fruit brunches, pine wood meal, lignocellulosic biomass, eucalyptus leaves, coconut fibers [22, 50]. Figure 1 (b) presents evolution of HHV versus severity factor for lavandin hydrochars and coconut fibers and eucalyptus leaves hydrochars from Liu et al. [47] for comparison. HHV values obtained at different severity factors for different kind of biomass and the same S:L initial condition, are of the same order of magnitude and ranged from 25 to 30 MJ kg^{-1}. Hence, calorific values for lavandin hydrochars are comparable with the ones for coconut fibers and eucalyptus leaves, indicating that lavandin hydrochars could be interesting solid fuel. From SF 4 to SF 5, HHV value remained constant irrespectively of SF value. Between SF 5 and SF 6, HHV value increased from 25 to 30 MJ kg^{-1}, then above SF 6, HHV value reached a plateau and remained constant whatever the SF value. In the case of lavandin hydrochars, HHV value evolution is directly

correlated to carbon content. The described trend was the same for coconut and eucalyptus hydrochars, with an increase of HHV for severity factor from 5 to 6, then above 6 HHV value did not change significantly and remained stable. In conclusion, regarding HHV value, hydrochars obtained for SF 6 seemed to be a good compromise. Figure 1 (c) presents evolution of hydrochar yield as a function of severity factor. Two distinct segments arose: the first one concerned severity factors from 4 to 6 where hydrochar yield strongly decreased with a slope near to 8%/SF unit; the second segment concerned severity factors above 6, where hydrochar yield decrease was slighter with a slope near to 2%/SF unit. Regarding optimal hydrochar yield, a severity factor around 6 seemed to be a good compromise for solid fuel application. Evolution of energy yield as a function of severity factor is presented Fig. 1 (d). In the range of severity factors studied, energy yield of lavandin hydrochars decreased from 68–53%, and the maximum value for energy yield corresponded to the sample obtained at the lowest severity factor value. Compared with energy yields for coconut fibers and eucalyptus leaves hydrochars [41], lavandin, coconut fibers, and eucalyptus hydrochars had energy yields in the same order of magnitude and depicted a linear decrease trend as severity factor increased and the rates of decay were similar. The rate of decay was similar for lavandin and coconut fibers hydrochars, whereas it was higher for eucalyptus leaves hydrochars, indicating that the latter were less interesting biofuels compared to lavandin and coconut fibers.

Table 2

Proximate and ultimate analysis of lavandin sample and its hydrochars. (*) Fuel ratio corresponds to the fixed carbon/volatile matter ratio; (**) HHV was calculated according to Channiwala et al. (2002) [38]; (****) Hydrochar yield (%) was calculated as $\frac{driedhydrocharweight}{driedbiomassweight} \times 100$; (***) Energy yield corresponds to $\frac{HHV_{hydrochar}}{HHV_{biomass}} \times hydrocharyield$

	L	LH1-220	LH2-220	LH4-220	LH8-220	LH20-220	LH4-180	LH4-200	LH4-240	LH20-200	LH20-240	LH20-260
Moisture (%)	2.93	0.68	0.65	0.51	0.42	0.4	1.21	1.06	0.39	0.65	0.39	0.33
Volatile matter (%)	80.89	72.66	70.28	67.08	63.6	60.67	70.19	74.96	61.65	65.54	58.43	54.91
Fixed carbon (%)	8.55	21.86	24.07	27.77	31.2	34.34	23.25	19.83	33.22	28.41	35.76	37.8
Ash (%)	7.63	4.8	5.0	4.64	4.78	4.59	5.35	4.15	4.74	5.4	5.42	6.96
Fuel ratio *	0.11	0.30	0.34	0.41	0.49	0.57	0.33	0.26	0.54	0.43	0.61	0.69
C (%)	50.77	60.42	61.54	64.98	67.24	70.1	58.79	61.35	69.65	65.31	71.94	71.59
H (%)	6.9	6.81	6.31	6.27	6.28	6.51	6.48	6.21	6.75	6.82	6.65	6.04
N (%)	1.28	1.09	1.18	1.31	1.44	1.62	1.29	1.24	1.53	1.46	1.69	1.77
O (%)	41.05	31.68	30.97	27.44	25.04	21.77	33.44	31.2	22.07	26.41	19.72	20.6
HHV (MJ/kg) **	21.43	25.72	25.59	27.12	28.16	29.77	24.57	25.40	29.86	27.97	30.77	29.81
Energy yield (%) ***	NA	65.15	61.05	60.31	55.59	56.36	68.26	64	57.75	66.51	58.11	53.63
Hydrochar yield (%) ****	NA	54.27	51.12	47.66	42.3	40.57	59.54	53.99	41.44	50.96	40.47	38.56

The atomic ratios H/C and O/C of lavandin and hydrochars are presented in Fig. 2, as Van Krevelen diagram, in order to compare biomass and hydrochars with fossil fuels. Lavandin sample showed worse quality than peat, but its hydrochars showed wide range quality between bituminous coal to peat. Pathways for dehydration, and decarboxylation are also illustrated. From Fig. 2, dehydration and decarboxylation were the two main biomass transformations during HTC, rather than demethylation that should depict a decrease of H/C atomic ratio with an increase of O/C atomic ratio [51]. Hydrochars presenting properties closer to bituminous coal and lignite when the ones obtained for HTC conditions with severity factors higher than 6, indicating that high temperature and high retention time increased the coalification process of biomass.

SEM and ATR-FTIR

The surface morphologies of raw lavandin and its corresponding hydrochars are visualized in Figs. 3 and 4. Because of using the blender to crush the lavandin without the HTC process, broken branches and broken flowers can be seen from Fig. 3 (a). In Fig. 4 (a), raw lavandin showed fibrous structure with a smooth surface which is the typical structure of herbaceous biomass [52].

After the HTC process, each hydrochar had different levels of decomposition. The flower part completely disappeared after the HTC process. Corresponding to different experimental conditions, a great quantity of large-sized fibrous structures in LH1-220, LH2-220, LH4-220, LH4-180 and LH4-200 were preserved (Fig. 3 (b, c, d, g, h)), whose severity factors were less than 6. Further hydrolysis of cellulose or hemicellulose and partial hydrolysis of lignin, with the increase in severity factor, LH8-220, LH20-220, LH4-240, and LH20-200 samples were dominated by heterogeneous fragments so that only a few fibrous structures were observable as shown in Fig. 3 (e, f, i, g) [53]. When the severity factors were larger than 7, which represented the hydrochars LH20-240 and LH20-260 (Fig. 3 (k, l)), the fibrous structures were completely decomposed and disappeared, the heterogeneous fragments were reorganized into coal-like carbon particles, and it showed melted and agglomerated structures.

The fibrous structures in hydrochars are shown in Fig. 4 (b-l). After the HTC process, the surface of fibrous structure became rough, even the LH4-180, which had the lowest severity factor, showed some wrinkles and cracks on the surface and the original shape of the fibrous structure has been preserved [54, 55]. After that, samples showed different degrees of decomposition depending on the experimental conditions. Overall, with the gradual increase in severity factors, the surface tended to be rough and decomposed step by step, the tubular structure as Fig. 4 (e, f) and skeleton structure as Fig. 4 (h) inside were revealed and further decomposed. Another manifestation of fibrous structure shrinking was that its diameter was greatly reduced as shown in Fig. 4 (i, j). As shown in Figs. 3 (k, l), when severity factors were 7.2 and 7.9, respectively, the reaction conditions were sufficiently severe. It caused that the fibrous structure was exhausted and replaced by dense particles after hydrothermal carbonization.

The particle size of each sample was measured and plotted as a distribution histogram shown in Fig. 5. Lavandin was mainly dominated by particles larger than 100 μm. Because of the degradation during the HTC reaction, a large number of particles smaller than 100 μm appeared in the hydrochars, and this proportion showed a trend of first increasing and then decreasing with the increase in severity factor. This trend can also be seen from the comparison of SEM images. As the HTC reaction progresses, large particles decomposed into smaller particles, and then small particles reorganized and aggregated into larger particles. Finally, when the severity factor was larger than 7, corresponding to samples LH20-240 and LH20-260, the particle size distribution was similar. A higher temperature could lead to a more uniform average diameter and uniform size distribution [56].

Comparative ATR-FTIR spectra of the raw lavandin and its corresponding hydrochars are shown in Fig. 6. The band at 3600–3000 cm^{-1} is attributed to the O-H stretching vibration in the hydroxyl or carboxyl groups [57]. When SF increased, especially when higher than 7, the intensity of the O-H stretching band decreased significantly, which indicates the results of dehydration and decarboxylation reactions during the HTC. The peaks at 2930 and 2850 cm^{-1} are ascribed to C-H stretching vibration in aromatic and aliphatic structure in lavandin and hydrochars[58]. The characteristic C = O stretching of carboxylic

acid groups in the hemicellulose appeared approximately at 1730 cm^{-1} in the spectra of raw lavandin. It disappeared in its corresponding hydrochars due to decomposition of hemicellulose [59, 60]. The peak at around 1700 cm^{-1} in all hydrochar samples is ascribed to the C = O groups in cellulose and lignin. When the temperature increased, relative intensification in this peak occurred due to the disappearance of the band at 1730 cm^{-1} corresponding to the C = O bond in hemicellulose. The intensification points out that the decomposition of hemicellulose occurred at lower temperature compared with cellulose and lignin [61, 57]. C = C stretching vibration is seen at 1600 and 1500 cm^{-1} and C-H bending vibration is seen at 1447 cm^{-1}, indicating the presence of mononuclear aromatic structures in L and all hydrochars. The aliphatic ether C-O stretching vibration is observable at 1160, 1100, 1060 and 1030 cm^{-1} [55, 62]. Although the exact mechanism of the HTC reactions is still being elucidated, it can still be inferred that dehydration, decarboxylation and hydrolysis reactions likely occured during the HTC process.

Combustion behavior and thermal properties of lavandin and hydrochars

Thermodegradation of lavandin sample and hydrochars was performed under constant air flow (150 mL min^{-1}) and constant heating rate (10°C min^{-1}), in order to evaluate the combustion behavior of the samples. TGA and DTG curves for lavandin (Fig. 7 (a)) and its hydrochars obtained after a short retention time (from 1 hour to 4 hours) (Fig. 7 (b) to (d)), or a low temperature (below 220°C) and a relatively short time (4 hours) (Fig. 7 (g and h)) depicted the same trend: at around 100°C water evaporation and sublimation of low molecular weight component occurred, followed by a first degradation stage between 200°C and 400°C attributed to devolatilization and combustion, and finally a second degradation stage between 400°C and 650°C attributed to degradation products (char) combustion [47]. Ornaghi et al. [63] demonstrated that during thermodegradation of lignocellulosic fibers, water, extractives, hemicellulose and cellulose were totally degraded at temperature above 400°C, lignin was totally degraded at temperature above 550°C. Degradation of lignin at higher temperature than cellulose and hemicellulose was attributed to its complex, cross-linked three dimensional aromatic polymer structure, compared to the linear structure of cellulose and branched and amorphous polymer structure of hemicellulose. Chars of hemicellulose and cellulose started to degrade at 300°C while lignin char started to degrade at 400°C. Considering the experimental conditions used to obtain hydrochars LH1-220, LH2-220, LH4-220, LH4-180, LH4-200, TG/DTG curves presenting a two stage degradation process confirmed that extractives, cellulose, hemicellulose and lignin were partially degraded during HTC process. The calculated severity factors for these hydrochars were very narrow, ranging from 4.74 to 5.91. Hence, the time-temperature combinations chosen for these samples provided approximatively the same kind of hydrochar, with comparable thermal properties. The calculated kinetic parameters are presented in Table 3. First order kinetic model gave the best correlation coefficients ranging from 0.93 to 0.99 for lavandin sample (L) and all its hydrochars. Considering the two thermodegradation stages appearing on TG/DTG curves for L, LH1-220 to LH20-220, LH4-180 and LH4-200, kinetic parameters were determined for each one of them (Table 3). Activation energy and pre-exponential factor for lavandin sample (L) were lower for both stages than LH1-220, LH2-220, LH4-220 hydrochars, indicating that L sample was more reactive to ignite than hydrochars obtained at 220°C. When retention time was increased to 8h or 20h and temperature was kept constant (220°C), activation energy and pre-exponential factor were lower than for lavandin sample, indicating that hydrochars were more reactive to ignite than lavandin. When retention time was kept constant (4h) and temperatures were lower than 220°C, the activation energy and pre-exponential factor were comparable to the ones obtained for LH1-220 to LH4-220. Regarding hydrochars obtained at temperatures larger than 220°C and/or retention time larger than or equal to 4h, distinction of several degradation stages is not as obvious as previously. TG/DTG curves depicted a single stage thermal decomposition covering a large temperature range from 200°C to 800°C, probably indicating that extractives, hemicellulose and cellulose were already totally or partially degraded during HTC process. TG/DTG curves may correspond (i) to a lesser extent to the thermal degradation of the remaining extractives, cellulose and hemicellulose and (ii) in a larger extent to chars degradation. Activation energy was around two times lower than for others hydrochars, indicating a good ignition, and pre-exponential factor was very low. In general, the pre-exponential factor gives values indicating the fraction of reactant molecules possessing enough kinetic energy to react. In the particular HTC process, its values are located in a wide

range as the thermal degradations occur in solid phase. As shown in Table 3, the A values are in the range 185.4–0.001 min^{-1}. It was noticeable that LH4-240, LH20-240, LH20-260 and LH20-220 hydrochars have the lowest values of A factor, signature of a surface reaction. The severity factor values for these hydrochars were higher than the previous ones (superior to 6), and the combination of time and temperature gave hydrochars with satisfactory thermal properties.

Table 3

Combustion kinetic parameters (E, A, n, R^2) of Lavandin (L) and its hydrochars (LH) obtained at different temperature and different retention time. Ignition temperature (T_i), maximum combustion rate temperature (T_m), and burnout temperature (T_b); S: combustibility index $= \frac{\left(\frac{dw}{dt}\right)_{max}\left(\frac{dw}{dt}\right)_{mean}}{T_b \times T_i^2}$, with $\left(\frac{dw}{dt}\right)_{max}$ and $\left(\frac{dw}{dt}\right)_{mean}$ the maximum and mean weight loss rate (%/min), respectively[64]

	SF	Temperature range (°C)	E (kJ/mol)	A (min^{-1})	n	R^2	T_i (°C)	T_b(°C)	S (10^{-8}) ($\%^2 min^{-2}\ °C^{-3}$)
L	NA	160–400	26.43	11.5	1	0.98	230	505	19.8
		400–540	38.46	100.7	1	0.94			
LH1-220	5.31	219–386	34.15	31.0	1	0.97	270	553	13.5
		386–590	43.66	165	1	0.95			
LH2-220	5.61	225–389	33.61	24.3	1	0.97	270	570	12.1
		389–595	43.37	132.8	1	0.94			
LH4-220	5.91	231–384	30.61	10.1	1	0.97	270	582	11.0
		384–610	45.87	185.4	1	0.95			
LH8-220	6.21	235–373	24.15	1.8	1	0.99	312	646	5.25
		373–685	39.22	36.3	1	0.95			
LH20-220	6.61	235–292	18.61	0.4	1	0.99	330	662	4.43
		292–692	32.87	10	1	0.95			
LH4-180	4.74	212–379	33.16	32.3	1	0.98	260	615	11.9
		379–664	30.16	12.3	1	0.98			
LH4-200	5.32	212–379	34.23	34.3	1	0.97	270	615	10.5
		379–664	34.22	24	1	0.93			
LH4-240	6.50	212–782	13.87	0.001	1	0.99	280	821	3.06
LH20-200	6.02	212–517	27.3	8.7	1	0.99	260	880	3.25
LH20-240	7.20	212–940	15.52	0.2	1	0.99	300	950	2.38
LH20-260	7.79	212–782	17.24	0.3	1	0.98	300	851	2.96

T_i and T_b (Table 3) obtained for lavandin sample (230°C and 505°C, respectively) were lower than T_i and T_b obtained for hydrochars (270°C to 330°C and 553 to 950°C, respectively), indicating that hydrochars were better biofuels than raw lavandin. Low T_i values is governed by the amount of volatile matter in the hydrochar: as high the volatile matter content is, as low T_i is. High ignition temperature indicated that hydrochars used as solid biofuels could be safely stored at ambient temperature and transported, without risk of auto-ignition. The highest T_i values corresponded to hydrochars obtained for a retention time superior to 8h at moderated HTC-temperature (180–220°C), or at high HTC-temperatures (240–260°C).

Burnout temperature increased as the retention time and/or the HTC-temperature increased. The highest T_b values were obtained at the highest HTC-temperature and the longest retention time (240–260°C; 20h). The increase of burnout temperature is correlated with the increase of fixed carbon measured in hydrochars. Longer the retention time during HTC (and/or higher temperature) is, more thermally stable the carbon components in hydrochars are.

Combustibility index is presented as a function of severity factor used during HTC experiments in Fig. 8. From this figure, differences in combustibility index clearly appeared as two groups of datasets: the first one corresponded to the combustibility index for hydrochars obtained at SF below 6, and the second one corresponded to the combustibility index for hydrochars obtained at SF above 6. For SF < 6, the combustibility index was two to three-fold superior to the combustibility index obtained for SF above 6, indicating that these hydrochars were more suitable for combustion purposes.

Conclusion

Lavandin distilled straws were submitted to hydrothermal carbonization under various temperature and retention time allowing to reach a severity factor range from 4.74 to 7.79. After the HTC process, the flower part of raw lavandin disappeared completely and the smooth fibrous structure was also decomposed. With the increase of SF, a large number of heterogeneous fragments appeared then recombined into coal-like particles, as well as the particle size distribution was gradually uniform. FTIR analysis indicated dehydration, decarboxylation and hydrolysis are expected to occur during the HTC process.

Hydrochars resulting from HTC showed lower proportion of volatile matter, ash and higher proportion of fixed carbon compared with raw lavandin. Consequently, the fuel ratio was significantly improved. HHV value increased from 21.43 MJ/kg for lavandin to a maximum of 30.77 MJ/kg for hydrochars. The ignition and burnout temperatures of raw lavandin were lower than hydrochars. Under SF 6, activation energy and pre-exponential factor for combustion of hydrochars were higher than raw lavandin. TGA results and calculated kinetic parameters indicated that hydrochars were less reactive to ignite and easier to store.

Taking into account the evolution of energy yield and hydrochar yield with temperature and retention time during the HTC process, the hydrochar obtained for SF around 6 had fuel properties close to bituminous coal and lignite. SF close to 6 was the best compromise for valorization of lavandin distilled straws as solid fuel by using HTC.

Based on the above results, lavandin hydrochars are expected to be solid fuels with excellent performances. It also provides an eco-friendly and economical valorization route for cosmetic plant residues.

Declarations

Acknowledgements:

Sumeyra Seniha Baran acknowledges Région Sud/Provence-Alpes-Côte d'Azur and the company Jyta for the financial support of her PhD fellowship, as well as Pôle innov'alliance. Xin Li warmly acknowledges China Scholarship Council (CSC) for their support through his PhD fellowship. Professor Pierre-Charles Maria is warmly acknowledged for providing lavandin samples.

Fundings:

This work received financial support of Région Sud/Provence-Alpes-Côte d'Azur and the company Jyta, China Scholarship Council (CSC) through PhD fellowships. The scanning electron microscope of the Centre Commun de Microscopie Appliquée (CCMA) was funded by the Région Sud/Provence-Alpes-Côte d'Azur and the Conseil Départemental des Alpes Maritimes. This work has also been supported by the French government, through the UCA^{JEDI} Investments in the Future project managed by the National Research Agency (ANR) with the reference number ANR-15-IDEX-01.

Competing interests:

The authors have no relevant financial or non-financial interests to disclose.

Author Contribution:

Xin Li and Sumeyra Seniha Baran have equally contributed to this work : sample preparation, material characterization, redaction of the manuscript under supervision of Claire Lomenech, Pavel Kuzhir and Charlotte Hurel. SEM picture were performed under supervision of François Orange. TGA analysis were performed under supervision of Alice Mija. Elemental analysis were performed by Erik Bonjour and Patrick Jame. All the authors read, commented, corrected the previous versions of the manuscript, and finally approved the final version of the manuscript.

Data availability:

The datasets generated during the current study are not publicly available due to confidentiality agreement, but are available from the corresponding author on reasonable request.

References

1. Lesage-Meessen L, Bou M, Sigoillot JC, Faulds CB, Lomascolo A (2015) Essential oils and distilled straws of lavender and lavandin: a review of current use and potential application in white biotechnology. Appl Microbiol Biotechnol. https://doi.org/10.1007/s00253-015-6511-7
2. Saha A, Basak BB (2020) Scope of value addition and utilization of residual biomass from medicinal and aromatic plants. Ind Crops Prod. https://doi.org/10.1016/j.indcrop.2019.111979
3. Briens C, Piskorz J, Berruti F (2008) Biomass valorization for fuel and chemicals production–A review. Int J Chem. https://doi.org/10.2202/1542-6580.1674
4. Grifoni M, Pedron F, Barbafieri M, Rosellini I, Petruzzelli G, Franchi E (2021) : Sustainable valorization of biomass: from assisted phytoremediation to green energy production. Handbook of Assisted and Amendment: Enhanced Sustainable Remediation Technology. https://doi.org/10.1002/9781119670391.ch2
5. Alavi-Borazjani SA, Capela I, Tarelho LAC (2020) Valorization of biomass ash in biogas technology: Opportunities and challenges. Energy Rep. https://doi.org/10.1016/j.egyr.2019.09.010
6. Kapoor R, Ghosh P, Kumar M, Sengupta S, Gupta A, Kumar SS, Vijay V, Kumar V, Kumar Vijay V, Pant D (2020) Valorization of agricultural waste for biogas based circular economy in India: a research outlook. Bioresour Technol. https://doi.org/10.1016/j.biortech.2020.123036
7. Volf I, Rakoto NG, Bulgariu L (2015) Valorization of Pistia stratiotes biomass as biosorbent for lead (II) ions removal from aqueous media. Sep Sci Technol. https://doi.org/10.1080/01496395.2014.978018
8. Agarwal A, Upadhyay U, Sreedhar I, Singh SA, Patel CM (2020) A review on valorization of biomass in heavy metal removal from wastewater. J Water Process Eng. https://doi.org/10.1016/j.jwpe.2020.101602
9. Foong SY, Liew RK, Yang Y, Cheng YW, Yek PNY, Mahari WAW, Lee XY, Han CS, Vo D-VN, Le QV, Aghbashlo M, Tabatabaei M, Sonne C, Peng W, Lam SS (2020) Valorization of biomass waste to engineered activated biochar by microwave pyrolysis: progress, challenges, and future directions. Chem Eng J. https://doi.org/10.1016/j.cej.2020.124401
10. Lomenech C, Hurel C, Messina L, Schembri M, Tosi P, Orange F, Georgi F, Mija A, Kuzhir P (2021) A Humins-Derived Magnetic Biochar for Water Purification by Adsorption and Magnetic Separation. Waste Biomass Valor. https://doi.org/10.1007/s12649-021-01481-3
11. Rodríguez P, Cerda A, Font X, Sánchez A, Artola A (2019) Valorisation of biowaste digestate through solid state fermentation to produce biopesticides from Bacillus thuringiensis. Waste Manag. https://doi.org/10.1016/j.wasman.2019.05.026

12. Singh G, Tiwari A, Rathore H, Prasad S, Hariprasad P, Sharma S (2021) Valorization of paddy straw using de-oiled cakes for P. ostreatus cultivation and utilization of spent mushroom substrate for biopesticide development. Waste Biomass Valor. https://doi.org/10.1007/s12649-020-00957-y
13. Das SK, Ghosh GK, Avasthe R (2020) Valorizing biomass to engineered biochar and its impact on soil, plant, water, and microbial dynamics: a review. Biomass Conv Bioref. https://doi.org/10.1007/s13399-020-00836-5
14. Braghiroli FL, Passarini L (2020) Valorization of biomass residues from forest operations and wood manufacturing presents a wide range of sustainable and innovative possibilities. Curr Forestry Rep. https://doi.org/10.1007/s40725-020-00112-9
15. Koul B, Yakoob M, Shah MP (2021) Agricultural waste management strategies for environmental sustainability. Environ Res. https://doi.org/10.1016/j.envres.2021.112285
16. Giannetto A, Oliva S, Riolo K, Savastano D, Parrino V, Cappello T, Maisano M, Fasulo S, Mauceri A (2020) Waste valorization via Hermetia illucens to produce protein-rich biomass for feed: Insight into the critical nutrient taurine. Animals. https://doi.org/10.3390/ani10091710
17. Lesage-Meessen L, Bou M, Ginies C, Chevret D, Navarro D, Drula E, Bonnin E, del Rio JC, Odinot E, Bisotto A, Berrin J-G, Sigoillot J-C, Faulds CB, Lomascolo A (2018) Lavender-and lavandin-distilled straws: an untapped feedstock with great potential for the production of high-added value compounds and fungal enzymes. Biotechnol Biofuels. https://doi.org/10.1186/s13068-018-1218-5
18. Angelova G, Brazkova M, Stefanova P, Blazheva D, Vladev V, Petkova N, Slavov A, Denev P, Karashanova D, Zaharieva R, Enev A, Krastanov A (2021) Waste Rose Flower and Lavender Straw Biomass—An Innovative Lignocellulose Feedstock for Mycelium Bio-Materials Development Using Newly Isolated Ganoderma resinaceum GA1M. J Fungi. https://doi.org/10.3390/jof7100866
19. Greff B, Szigeti J, Varga Á, Lakatos E, Sáhó A, Varga L (2021) Effect of bacterial inoculation on co-composting of lavender (Lavandula angustifolia Mill.) waste and cattle manure. 3 Biotech. https://doi.org/10.1007/s13205-021-02860-2
20. Owsianiak M, Ryberg MW, Renz M, Hitzl M, Hauschild MZ (2016) Environmental performance of hydrothermal carbonization of four wet biomass waste streams at industry-relevant scales. ACS Sustainable Chem Eng. https://doi.org/10.1021/acssuschemeng.6b01732
21. Pauline AL, Joseph K (2020) Hydrothermal carbonization of organic wastes to carbonaceous solid fuel–A review of mechanisms and process parameters. Fuel. https://doi.org/10.1016/j.fuel.2020.118472
22. Nizamuddin S, Baloch HA, Griffin GJ, Mubarak NM, Bhutto AW, Abro R, Mazari SA, Ali BS (2017) An overview of effect of process parameters on hydrothermal carbonization of biomass. Renew Sust Energ Rev. https://doi.org/10.1016/j.rser.2016.12.122
23. Xiao LP, Shi ZJ, Xu F, Sun RC (2012) Hydrothermal carbonization of lignocellulosic biomass. Bioresour Technol. https://doi.org/10.1016/j.biortech.2012.05.060
24. Hoekman SK, Broch A, Robbins C (2011) Hydrothermal carbonization (HTC) of lignocellulosic biomass. Energy Fuels. https://doi.org/10.1021/ef101745n
25. Oliveira I, Blöhse D, Ramke HG (2013) Hydrothermal carbonization of agricultural residues. Biores Technol. https://doi.org/10.1016/j.biortech.2013.04.125
26. Heilmann SM, Davis HT, Jader LR, Lefebvre PA, Sadowsky MJ, Schendel FJ, von Keitz MG, Valentas KJ (2010) Hydrothermal carbonization of microalgae. Biomass Bioenerg. https://doi.org/10.1016/j.biombioe.2010.01.032
27. Wüst D, Correa CR, Suwelack KU, Köhler H, Kruse A (2019) Hydrothermal carbonization of dry toilet residues as an added-value strategy–Investigation of process parameters. J Environ Manage. https://doi.org/10.1016/j.jenvman.2019.01.005

28. Lang Q, Chen M, Guo Y, Liu Z, Gai C (2019) Effect of hydrothermal carbonization on heavy metals in swine manure: speciation, bioavailability and environmental risk. J Environ Manage. https://doi.org/10.1016/j.jenvman.2018.12.073
29. Basso D, Patuzzi F, Castello D, Baratieri M, Rada EC, Weiss-Hortala E, Fiori L (2016) Agro-industrial waste to solid biofuel through hydrothermal carbonization. Waste manag. https://doi.org/10.1016/j.wasman.2015.05.013
30. Yao Z, Ma X (2018) Characteristics of co-hydrothermal carbonization on polyvinyl chloride wastes with bamboo. Bioresour Technol. https://doi.org/10.1016/j.biortech.2017.09.098
31. Saba A, Saha P, Reza MT (2017) : Co-Hydrothermal Carbonization of coal-biomass blend: Influence of temperature on solid fuel properties. Fuel Process. Technol. https://doi.org/10.1016/j.fuproc.2017.08.016
32. Overend RP, Chornet E (1987) Fractionation of lignocellulosics by steam-aqueous pretreatments. Philos Trans Royal Soc A. https://doi.org/10.1098/rsta.1987.0029
33. Chen SF, Mowery RA, Chambliss CK, van Walsum GP (2007) Pseudo reaction kinetics of organic degradation products in dilute-acid-catalyzed corn stover pretreatment hydrolysates. Biotechnol Bioeng. https://doi.org/10.1002/bit.21480
34. Chum HL, Johnson DK, Black SK, Overend RP (1990) Pretreatment-catalyst effects and the combined severity parameter. Appl Biochem Biotechnol. https://doi.org/10.1007/BF02920229
35. American Society for Testing and Materials (ASTM) (2013) E871-82 Standard test method for moisture analysis of particulate wood fuels. Annual book of ASTM Standard, American Society for Testing and Materials
36. American Society for Testing and Materials (ASTM) (2015) E1755-01 Standard test method for ash in biomass. Annual book of ASTM Standard, American Society for Testing and Materials
37. American Society for Testing and Materials (ASTM) (2013) E872-82 Standard test method for volatile matter in the analysis of particulate wood fuels. Annual book of ASTM Standard, American Society for Testing and Materials
38. Channiwala SA, Parikh PP (2002) A unified correlation for estimating HHV of solid, liquid and gaseous fuels. Fuel. https://doi.org/10.1016/S0016-2361(01)00131-4
39. Schneider CA, Rasband WS, Eliceiri KW (2012) NIH Image to ImageJ: 25 years of image analysis. Nat Methods. .https://doi.org/10.1038/nmeth.2089
40. Lu JJ, Chen WH (2015) Investigation on the ignition and burnout temperatures of bamboo and sugarcane bagasse by thermogravimetric analysis. Appl Energy. https://doi.org/10.1016/j.apenergy.2015.09.026
41. Liu Z, Quek A, Hoekman SK, Balasubramanian R (2013) Production of solid biochar fuel from waste biomass by hydrothermal carbonization. Fuel. https://doi.org/10.1016/j.fuel.2012.07.069
42. Peng C, Zhai Y, Zhu Y, Xu B, Wang T, Li C, Zeng G (2016) Production of char from sewage sludge employing hydrothermal carbonization: char properties, combustion behavior and thermal characteristics. Fuel. https://doi.org/10.1016/j.fuel.2016.02.068
43. Coats AW, Redfern JP (1964) Kinetic parameters from thermogravimetric data. Nature. https://doi.org/10.1038/201068a0
44. Samuelsson R, Burvall J, Jirjis R (2006) Comparison of different methods for the determination of moisture content in biomass. Biomass Bioenerg. https://doi.org/10.1016/j.biombioe.2006.06.004
45. Nakason K, Panyapinyopol B, Kanokkantapong V, Viriya-empikul N, Kraithong W, Pavasant P (2018) Hydrothermal carbonization of unwanted biomass materials: Effect of process temperature and retention time on hydrochar and liquid fraction. J Energy Inst. https://doi.org/10.1016/j.joei.2017.05.002
46. Park KY, Lee K, Kim D (2018) Characterized hydrochar of algal biomass for producing solid fuel through hydrothermal carbonization. Biores Technol. https://doi.org/10.1016/j.biortech.2018.03.003
47. Liu Z, Quek A, Hoekman SK, Balasubramanian R (2013) Production of solid biochar fuel from waste biomass by hydrothermal carbonization. Fuel. https://doi.org/10.1016/j.fuel.2012.07.069
48. He C, Giannis A, Wang JY (2013) Conversion of sewage sludge to clean solid fuel using hydrothermal carbonization: hydrochar fuel characteristics and combustion behavior. Appl Energy. https://doi.org/10.1016/j.apenergy.2013.04.084

49. Peng C, Zhai Y, Zhu Y, Xu B, Wang T, Li C, Zeng G (2016) Production of char from sewage sludge employing hydrothermal carbonization: char properties, combustion behavior and thermal characteristics. Fuel. .https://doi.org/10.1016/j.fuel.2016.02.068
50. Sharma HB, Sarmah AK, Dubey B (2020) Hydrothermal carbonization of renewable waste biomass for solid biofuel production: A discussion on process mechanism, the influence of process parameters, environmental performance and fuel properties of hydrochar. Renew Sust Energy Rev. https://doi.org/10.1016/j.rser.2020.109761
51. Saetea P, Tippayawong N (2013) Recovery of value-added products from hydrothermal carbonization of sewage sludge. ISRN Chem Eng. http://dx.doi.org/10.1155/2013/268947
52. Cai J, Li B, Chen C, Wang J, Zhao M, Zhang K (2016) Hydrothermal carbonization of tobacco stalk for fuel application. Biores Technol. https://doi.org/10.1016/j.biortech.2016.08.098
53. Guo S, Dong X, Wu T, Shi F, Zhu C (2015) Characteristic evolution of hydrochar from hydrothermal carbonization of corn stalk. J Anal Appl Pyrolysis. https://doi.org/10.1016/j.jaap.2015.10.015
54. Khan T, Saud A, Jamari S, Rahim M, Park J, Kim H (2019) Hydrothermal carbonization of lignocellulosic biomass for carbon rich material preparation: A review. Biomass Bioenerg. https://doi.org/10.1016/j.biombioe.2019.105384
55. Guardia L, Suárez L, Querejeta N, Pevida C, Centeno T (2018) Winery wastes as precursors of sustainable porous carbons for environmental applications. J Clean Prod. https://doi.org/10.1016/j.jclepro.2018.05.085
56. Falco C, Baccile N, Titirici M (2011) Morphological and structural differences between glucose, cellulose and lignocellulosic biomass derived hydrothermal carbons. Green Chem. .https://doi.org/10.1039/C1GC15742F
57. Lin Y, Ma X, Peng X, Yu Z (2016) A Mechanism Study on Hydrothermal Carbonization of Waste Textile. Energy Fuels. https://doi.org/10.1021/acs.energyfuels.6b01365
58. Gao P, Zhou Y, Meng F, Zhang Y, Liu Z, Zhang W, Xue G (2016) Preparation and characterization of hydrochar from waste eucalyptus bark by hydrothermal carbonization. Energy. https://doi.org/10.1016/j.energy.2015.12.123
59. Petrovi L J, Peri i L N, Maksimovi L J, Maksimovi L V, Kragovi L M, Stojanovi L M, Lau evi L M, Mihajlovi M (2016) Hydrothermal conversion of grape pomace: Detailed characterization of obtained hydrochar and liquid phase. J Anal Appl Pyrolysis. https://doi.org/10.1016/j.jaap.2016.02.010
60. Nakason K, Panyapinyopol B, Kanokkantapong V, Viriya-empikul N, Kraithong W, Pavasant P (2018) Hydrothermal carbonization of unwanted biomass materials: Effect of process temperature and retention time on hydrochar and liquid fraction. J Energy Inst. https://doi.org/10.1016/j.joei.2017.05.002
61. Kabakcı S (2019) Pyrolysis and combustion characteristics and kinetics of wood sawdust and wood sawdust hydrochar. Environ Prog Sustain Energy. https://doi.org/10.1002/ep.13315
62. Zhu G, Yang L, Gao Y, Xu J, Chen H, Zhu Y, Wang Y, Liao C, Lu C, Zhu C, Fuel (2019) https://doi.org/10.1016/j.fuel.2019.02.039
63. Ornaghi HL, Ornaghi FG, Neves RM, Monticeli F, Bianchi O (2020) Mechanisms involved in thermal degradation of lignocellulosic fibers: a survey based on chemical composition. Cellulose. https://doi.org/10.1007/s10570-020-03132-7
64. Huang X, Jiang X, Han X, Wang H (2008) Combustion characteristics of fine-and micro-pulverized coal in the mixture of O_2/CO_2. Energy Fuels. https://doi.org/10.1021/ef800444c

Figures

Figure 1

Evolution of (a) Fuel ratio; (b) HHV, %C, %O, %H, %N; (c) Hydrochar yield; (d) Energy yield as a function of severity factor

Figure 2

Van Krevelen diagram for lavandin biomass and hydrochars

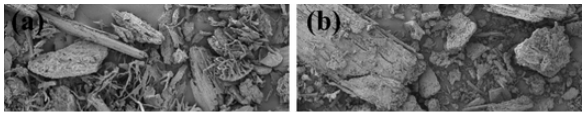

Figure 3

SEM images of lavandin and its corresponding hydrochars at 250x magnification: (a) L, (b) LH1-220, (c) LH2-220, (d) LH4-220, (e) LH8-220, (f) LH20-220, (g) LH4-180, (h) LH4-200, (i) LH4-240, (j) LH20-200, (k) LH20-240, (l) LH20-260

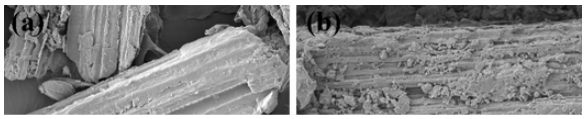

Figure 4

SEM images of lavandin and its corresponding hydrochars at 1500x magnification: (a) L, (b) LH1-220, (c) LH2-220, (d) LH4-220, (e) LH8-220, (f) LH20-220, (g) LH4-180, (h) LH4-200, (i) LH4-240, (j) LH20-200, (k) LH20-240, (l) LH20-260

Figure 5

Statistics of particle size distribution

Figure 6

ATR-FTIR spectra of lavandin and its corresponding hydrochars

Figure 7

TGA and DTG curves of thermodegradation under air of (a) Lavandin sample, and its hydrochars: (b) LH1-220, (c) LH2-220, (d) LH4-220, (e) LH8-220, (f) LH20-220, (g) LH4-180, (h) LH4-200, (i) LH4-240, (j) LH20-200, (k) LH20-240 and (l) LH20-260

Figure 8

Combustibility index (S) as a function of severity factor